Two-domain description of solute transport in heterogeneous porous media: Comparison between theoretical predictions and numerical experiments

F. Cherblanc [a,*], A. Ahmadi [b], M. Quintard [c]

[a] *LMGC – Cc 048, Université Montpellier 2, Place Eugène Bataillon, 34095 Montpellier Cedex, France*
[b] *TREFLE, Esplanade des Arts et Métiers, 33405 Talence Cedex, France*
[c] *Institut de Mécanique des Fluides, Allée du Prof. C. Soula, 31400 Toulouse, France*

Abstract

This paper deals with two-equation models describing solute transport in highly heterogeneous porous systems and more particularly dual permeability structures composed of high- and low-permeability regions. A macroscopic two-equation model has been previously proposed in the literature based on the *volume averaging technique* [Ahmadi A, Quintard M, Whitaker S. Transport in chemically and mechanically heterogeneous porous media V: two-equation model for solute transport with adsorption, Adv Water Resour 1998;22:59–86; Cherblanc F, Ahmadi A, Quintard M. Two-medium description of dispersion in heterogeneous porous media: calculation of macroscopic properties. Water Resour Res 2003;39(6):1154–73]. Through this theoretical upscaling method, both convection and dispersion mechanisms are taken into account in *both regions*, allowing one to deal with a large range of heterogeneous systems.

In this paper, the numerical tools associated with this model are developed in order to test the theory by comparing macroscopic concentration fields to those obtained by Darcy-scale numerical experiments. The heterogeneous structures considered are made up of low-permeability nodules embedded in a continuous high-permeability region. Several permeability ratios are used, leading to very different macroscopic behaviours. Taking advantage of the Darcy-scale simulations, the role of convection and dispersion in the mass exchange between the two regions is investigated.

Large-scale averaged concentration fields and elution curves are extracted from the Darcy-scale numerical experiments and compared to the theoretical predictions given by the two-equation model. Very good agreement is found between experimental and theoretical results. A permeability ratio around 100 presents a behaviour characteristic of ''mobile–mobile'' systems emphasizing the relevance of this two-equation description. Eventually, the theory is used to set-up a criterion for the existence of local equilibrium conditions. The potential importance of local-scale dispersion in reducing large-scale dispersion is highlighted. The results also confirm that a non-equilibrium description may be necessary in such systems, even if local-equilibrium behaviour could be observed.

Keywords: Porous media; Heterogeneous; Solute transport; Dispersion; Mass transfer; Two-equation model; Mobile-mobile; Nodular system

1. Introduction

The large spatial variability of hydraulic conductivity plays a major role in groundwater solute transport. These heterogeneities over a wide range of length scales usually lead to anomalous dispersion at the field-scale. Since only a limited amount of data is generally available, these heterogeneities in physical characteristics are often described through a geostatistical approach. With such a description, flow and transport reflect the uncertainty associated with the geological model. Within this general stochastic framework, two different approaches are used.

* Corresponding author. Tel.: +33 467 149 639; fax: +33 467 144 555.
E-mail address: chb@lmgc.univ-montp2.fr (F. Cherblanc).

Nomenclature

$A_{\eta\omega}$	area of the boundary between the η and the ω-region contained in the large-scale averaging volume V_∞, m^2
$\mathbf{b}_{\eta\eta}$	vector fields that maps $\nabla\{\langle c\rangle_\eta^\beta\}^\eta$ onto $\tilde{c}_\eta$, m
$\mathbf{b}_{\eta\omega}$	vector fields that maps $\nabla\{\langle c\rangle_\omega^\beta\}^\omega$ onto $\tilde{c}_\eta$, m
$\mathbf{b}_{\omega\eta}$	vector fields that maps $\nabla\{\langle c\rangle_\eta^\beta\}^\eta$ onto $\tilde{c}_\omega$, m
$\mathbf{b}_{\omega\omega}$	vector fields that maps $\nabla\{\langle c\rangle_\omega^\beta\}^\omega$ onto $\tilde{c}_\omega$, m
C^*	large-scale average concentration associated with a one-equation model, mol m^{-3}
$\langle c\rangle_\eta^\beta$	Darcy-scale intrinsic average concentration in the η-region, mol m^{-3}
$\langle c\rangle_\omega^\beta$	Darcy-scale intrinsic average concentration in the ω-region, mol m^{-3}
$\{\langle c\rangle_\eta^\beta\}^\eta$	large-scale intrinsic average concentration in the η-region, mol m^{-3}
$\{\langle c\rangle_\omega^\beta\}^\omega$	large-scale intrinsic average concentration in the ω-region, mol m^{-3}
$\tilde{c}_\eta$	spatial deviation concentration in the η-region, mol m^{-3}
$\tilde{c}_\omega$	spatial deviation concentration in the ω-region, mol m^{-3}
D^{eff}	Darcy-scale effective diffusivity, $m^2\ s^{-1}$
$\mathbf{D}^*$	Darcy-scale dispersion tensor, $m^2\ s^{-1}$
$\mathbf{D}_\eta^*$	Darcy-scale dispersion tensor in the η-region, $m^2\ s^{-1}$
$\mathbf{D}_\omega^*$	Darcy-scale dispersion tensor in the ω-region, $m^2\ s^{-1}$
$\widetilde{\mathbf{D}}_\eta$	spatial deviation of the dispersion tensor in the η-region, $m^2\ s^{-1}$
$\widetilde{\mathbf{D}}_\omega$	spatial deviation of the dispersion tensor in the ω-region, $m^2\ s^{-1}$
$\mathbf{D}_{\eta\eta}^{**}$	dominant dispersion tensor for the η-region transport equation, $m^2\ s^{-1}$
$\mathbf{D}_{\eta\omega}^{**}$	coupling dispersion tensor for the η-region transport equation, $m^2\ s^{-1}$
$\mathbf{D}_{\omega\omega}^{**}$	dominant dispersion tensor for the ω-region transport equation, $m^2\ s^{-1}$
$\mathbf{D}_{\omega\eta}^{**}$	coupling dispersion tensor for the ω-region transport equation, $m^2\ s^{-1}$
l	size of the unit cell, m
l_η	characteristic length associated with the η-region, m
l_ω	characteristic length associated with the ω-region, m
L	characteristic length associated with the large scale, m
l_i	lattice vectors, m
$\mathbf{n}_{\eta\omega}$	unit normal vector directed from the η-region towards the ω-region
r_η	scalar field that maps $(\{\langle c\rangle_\omega^\beta\}^\omega - \{\langle c\rangle_\eta^\beta\}^\eta)$ onto $\tilde{c}_\eta$
r_ω	scalar field that maps $(\{\langle c\rangle_\omega^\beta\}^\omega - \{\langle c\rangle_\eta^\beta\}^\eta)$ onto $\tilde{c}_\omega$
t	time, s
V_η	volume of the η-region contained in the averaging volume V_∞, m^3
V_ω	volume of the ω-region contained in the averaging volume V_∞, m^3
V_∞	large-scale averaging volume for the η–ω system, m^3
$\langle\mathbf{v}\rangle_\eta$	Darcy-scale filtration velocity in the η-region, m s^{-1}
$\{\langle\mathbf{v}\rangle_\eta\}^\eta$	intrinsic regional average velocity in the η-region, m s^{-1}
$\tilde{\mathbf{v}}_\eta$	spatial deviation for the filtration velocity in the η-region, m s^{-1}
$\langle\mathbf{v}\rangle_\omega$	Darcy-scale filtration velocity in the ω-region, m s^{-1}
$\{\langle\mathbf{v}\rangle_\omega\}^\omega$	intrinsic regional average velocity in the ω-region, m s^{-1}
$\tilde{\mathbf{v}}_\omega$	spatial deviation for the filtration velocity in the ω-region, m s^{-1}
$\{\langle\mathbf{v}\rangle\}$	superficial average velocity, m s^{-1}
α^*	mass exchange coefficient for the η–ω system, s^{-1}
α_{L}	Darcy-scale longitudinal dispersivity, m
α_{T}	Darcy-scale transversal dispersivity, m
δ_{ij}	Kronecker symbol
ε_η	total porosity in the η-region
ε_ω	total porosity in the ω-region
φ_η	volume fraction of the η-region
φ_ω	volume fraction of the ω-region
Θ	non-equilibrium criterion

The first approach entails a stochastic formulation of the flow equations, i.e., physical properties are represented as random variables. The resulting flow quantities are then also random variables, described in terms of expected values and higher statistical moments [3–7]. The second approach is a Monte Carlo methodology that requires the generation of multiple realizations of the heterogeneous formation. The transport problem is then considered from a "deterministic" point of view. In this second approach, the probability distribution of different quantities is determined through simulations over multiple realizations.

Indeed, using the second method, highly detailed geostatistical realizations are typically generated in order to capture all the scales of heterogeneity. Due to this high level of description, large-scale transport problems are computationally expensive (see an example in [8]). For this reason, some type of coarsening, or upscaling of the geologic model must be performed before it can be used for field-

scale numerical simulations. This upscaling is complicated by the fact that very fine-scale heterogeneities can have a major impact on simulation results, and these must be accurately accounted for in the macroscopic model.

Upscaling procedures are commonly used to coarsen these highly detailed geostatistical realizations to scales more suitable for the flow simulation. Examples of procedures available for the case of single-phase flow can be found in the literature [9–13]. In most cases, it is assumed that the macroscopic model represents the fine-scale heterogeneities contained in a grid block, while the large-scale heterogeneities are taken into account by the spatial discretization of the entire simulation. In the framework of solute transport, a non-ideal behavior, i.e., a non-Fickian response, may be observed at the field-scale [14–16], featuring an early breakthrough and a long tailing that cannot be represented by a classical advection-dispersion equation, i.e., a simple one-equation model. Interpretations of field-scale transport experiments usually reflect a scale-dependent dispersivity [17–21]. These phenomena are partly attributed to solute transfer between different regions with highly contrasted properties [22,23]. Some classes of such highly heterogeneous structures may often be represented by a simplified system constituted of two homogeneous porous media. In this bicontinuum model, the heterogeneous porous medium is represented by a high- and a low-permeable region. Two macroscopic concentrations are defined associated with each region. If solute transport characteristic times are relatively different in the two regions, a significant difference between these two large-scale concentrations is observed. This phenomenon is called *large-scale mass non-equilibrium*, and must be taken into account in large-scale transport models [24]. Two-medium descriptions, or two-equation models, are commonly used to represent these processes. Even with complex systems like natural formations, this approach proved to be useful in many practical situations [25–29]. Usually, convection and dispersion are neglected in the less permeable zone, which is called ''immobile'' zone. Only the exchange of mass with the more permeable zone, ''mobile'' zone, is considered. To represent this mass transfer, some mixed models can be generated by coupling an averaged description of the flow in the ''mobile'' zone with a local-scale detailed description of the Fickian diffusive transport in the ''immobile'' zone considered, most often and for simplicity reasons, as rectangular, cylindrical or spherical aggregates [30–33]. An alternative is to approximate this mass exchange by a first-order kinetic [22,34–41]. Indeed, it is well-known that this mass exchange is a transient phenomenon and that it may exhibit memory effects. Therefore, limitations of the first-order kinetic models may be unacceptable in some circumstances. To catch most of the characteristic times involved during the exchange of mass in complex heterogeneous structures, multiple-rate mass transfer models [42–44], or fractal developments [45] were proposed.

If the permeability contrast between the different zones is less important, advection may become significant in the less permeable zone, and several works have shown the relevance of taking this effect into account [46–48]. Following this idea, the two-equation models were revisited to take into account convection and dispersion mechanisms in both regions [1,40,49–56]. These models are often called ''mobile–mobile'' models.

One of the crucial problems encountered when using two-equation models is the determination of the large-scale ''effective'' properties embedded in the model. For idealized cases, some *a priori* estimates of the mass exchange coefficient have been proposed [35,57,53]. Numerical simulation of local-scale transport can be used to evaluate macroscopic properties [46,48,58]. However, in general, these properties are interpreted from experimental data. With this approach, macroscopic properties of a heterogeneous sample are obtained using a curve-fitting procedure [59–63]. Recently, Ahmadi et al. [1] derived a two-equation model using the *large-scale volume averaging method*. This method provides three closure problems that give an *explicit* link between the different scales, and makes it possible to determine directly the macroscopic properties associated with any heterogeneous double-permeability system. Cherblanc et al. [2] proposed an original numerical procedure to solve these three closure problems. The developed tools were used to discuss the influence of the local-scale characteristics on the large-scale properties, in the case of a nodular system. The theory was tested favorably in Ahmadi et al. [1] in the case of stratified systems. The purpose of this paper is to emphasize the ability of the proposed two-equation model to represent the non-ideal behavior of more general heterogeneous systems.

The scope of the paper is limited to the comparison between theoretical predictions and numerical experiments. For readability of the paper, the basic ideas of the volume averaging technique used to derive the two-equation model are summarized in the next section. The aim of Section 3 is to make a comparison between the theoretical predictions obtained from the present large-scale model and some reference solutions. These reference solutions are built using transport simulations performed at the local-scale or Darcy-scale, i.e., using a fine discretization of the heterogeneities. The numerical procedure used for the large-scale transport simulation is described. Finally, some comparisons are presented and the quality of the two-equation description is discussed. In the last section, the possible existence of non-equilibrium conditions for nodular systems is investigated numerically as a function of the system permeability and dispersivity ratios. Using the large-scale representation given by the two-equation model, the concentration difference between the two regions can be computed from very small to very large times, allowing us to analyze in detail the behavior of the system.

2. Theoretical background

The flow of a tracer is considered in a double-permeability system, as illustrated in Fig. 1. At the local-scale or Darcy-scale, the problem is entirely defined by the following equations [64–66]:

$$\varepsilon_\eta \frac{\partial \langle c\rangle_\eta^\beta}{\partial t} + \langle \mathbf{v}\rangle_\eta \cdot \nabla \langle c\rangle_\eta^\beta = \nabla \cdot (\mathbf{D}_\eta^* \cdot \nabla \langle c\rangle_\eta^\beta) \quad \text{in the } \eta\text{-region} \tag{1}$$

$$B.C.1 \quad \langle c\rangle_\eta^\beta = \langle c\rangle_\omega^\beta \quad \text{at } A_{\eta\omega} \tag{2}$$

$$B.C.2 \quad \mathbf{n}_{\eta\omega} \cdot (\mathbf{D}_\eta^* \cdot \nabla \langle c\rangle_\eta^\beta) = \mathbf{n}_{\eta\omega} \cdot (\mathbf{D}_\omega^* \cdot \nabla \langle c\rangle_\omega^\beta) \quad \text{at } A_{\eta\omega} \tag{3}$$

$$\varepsilon_\omega \frac{\partial \langle c\rangle_\omega^\beta}{\partial t} + \langle \mathbf{v}\rangle_\omega \cdot \nabla \langle c\rangle_\omega^\beta = \nabla \cdot (\mathbf{D}_\omega^* \cdot \nabla \langle c\rangle_\omega^\beta) \quad \text{in the } \omega\text{-region} \tag{4}$$

where $\langle c\rangle_\eta^\beta$ represents the intrinsic averaged concentration in the η-region, while $\langle \mathbf{v}\rangle_\eta$ represents the filtration velocity. The choice of the tracer case implies that velocity fields are obtained independently from the tracer transport problem. The one-phase flow problem received a lot of attention in the literature, and, in particular, the introduction of large-scale regional velocities, which is relevant to our study, are discussed by Quintard and Whitaker [67]. One of the difficulties of the subsequent upscaling is that the dispersion tensors, $\mathbf{D}_\eta^*$ and $\mathbf{D}_\omega^*$, are position and velocity-dependent.

The complete procedure for upscaling the transport equations that led to the two-equation model are discussed elsewhere [1,24]. Consequently, only the basic ideas are summarized in this paper. The volume averaging operator is defined as

$$\{\langle \psi\rangle_\alpha\} = \varphi_\alpha \{\langle \psi\rangle_\alpha\}^\alpha = \frac{1}{V_\infty} \int_{V_\alpha} \langle \psi\rangle_\alpha \, \mathrm{d}V \tag{5}$$

where φ_α represents the volume fraction of the α-region given by

$$\varphi_\alpha = \frac{V_\alpha}{V_\infty} \tag{6}$$

Volume averaged equations are generated by expressing any local-scale quantity associated with the α-region, $\langle \psi\rangle_\alpha$, as the sum of the associated volume averaged large-scale quantity, $\{\langle \psi\rangle_\alpha\}^\alpha$, and a fluctuating component, $\tilde{\psi}_\alpha$, [68–70]; i.e., we have

$$\langle \psi\rangle_\alpha = \{\langle \psi\rangle_\alpha\}^\alpha + \tilde{\psi}_\alpha \tag{7}$$

On the basis of these definitions and using large-scale averaging theorems, mathematical developments can be performed. The large-scale averaging technique calculates the transport equations and the effective properties at a given scale by an averaging process over the equations corresponding to the lower scale. Several assumptions have to be introduced: separation of scales and the possibility of locally representing the medium by a periodic system. This last assumption means that, at a given point, the system is entirely characterized by a single unit cell as complex as necessary, to keep all the problem features.

Within the framework of the volume averaging theory, the periodic assumption has given reasonable results, even for disordered media [8,71]. Moreover Pickup et al. [72] compared several numerical approaches for the calculation of effective permeability, their overall conclusion was that the most accurate and robust boundary conditions to perform upscaling was periodicity.

The large-scale mass non-equilibrium condition corresponds to processes in which large-scale concentrations are significantly different for the two regions, thus calling for a two-medium representation. Under some length-scale and time-scale constraints, a first-order development in term of the large-scale concentration difference leads to

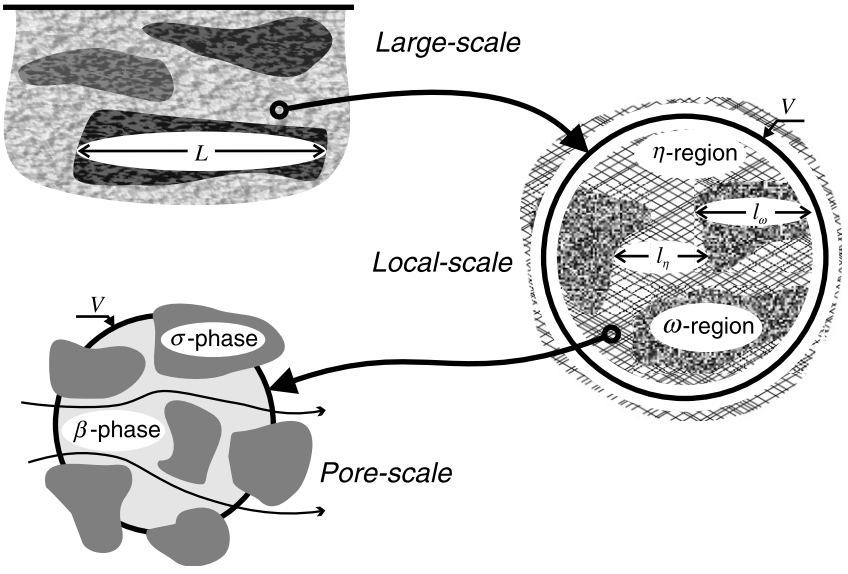

Fig. 1. The three scales of the problem: the pore-scale composed of a solid phase (σ) and a fluid phase (β); the local-scale consists of two embedded homogeneous regions (η and ω); the large-scale that still presents some macroscopic heterogeneities.

the following set of two large-scale equations [1,24]. In the η-region, we have

$$\varepsilon_\eta \varphi_\eta \frac{\partial \{\langle c\rangle_\eta^\beta\}^\eta}{\partial t} + \varphi_\eta \{\langle \mathbf{v}\rangle_\eta\}^\eta \cdot \nabla \{\langle c\rangle_\eta^\beta\}^\eta - \nabla \cdot \left[\mathbf{d}_\eta (\{\langle c\rangle_\eta^\beta\}^\eta - \{\langle c\rangle_\omega^\beta\}^\omega)\right] - \mathbf{u}_{\eta\eta} \cdot \nabla \{\langle c\rangle_\eta^\beta\}^\eta - \mathbf{u}_{\eta\omega} \cdot \nabla \{\langle c\rangle_\omega^\beta\}^\omega = \nabla \cdot \left[\mathbf{D}_{\eta\eta}^{**} \cdot \nabla \{\langle c\rangle_\eta^\beta\}^\eta\right] + \nabla \cdot \left[\mathbf{D}_{\eta\omega}^{**} \cdot \nabla \{\langle c\rangle_\omega^\beta\}^\omega\right] - \alpha^* \left(\{\langle c\rangle_\eta^\beta\}^\eta - \{\langle c\rangle_\omega^\beta\}^\omega\right) \tag{8}$$

while the large-scale equation for the ω-region is

$$\varepsilon_\omega \varphi_\omega \frac{\partial \{\langle c\rangle_\omega^\beta\}^\omega}{\partial t} + \varphi_\omega \{\langle \mathbf{v}\rangle_\omega\}^\omega \cdot \nabla \{\langle c\rangle_\omega^\beta\}^\omega - \nabla \cdot \left[\mathbf{d}_\omega (\{\langle c\rangle_\omega^\beta\}^\omega - \{\langle c\rangle_\eta^\beta\}^\eta)\right] - \mathbf{u}_{\omega\omega} \cdot \nabla \{\langle c\rangle_\omega^\beta\}^\omega - \mathbf{u}_{\omega\eta} \cdot \nabla \{\langle c\rangle_\eta^\beta\}^\eta = \nabla \cdot \left[\mathbf{D}_{\omega\omega}^{**} \cdot \nabla \{\langle c\rangle_\omega^\beta\}^\omega\right] + \nabla \cdot \left[\mathbf{D}_{\omega\eta}^{**} \cdot \nabla \{\langle c\rangle_\eta^\beta\}^\eta\right] - \alpha^* \left(\{\langle c\rangle_\omega^\beta\}^\omega - \{\langle c\rangle_\eta^\beta\}^\eta\right) \tag{9}$$

All large-scale effective properties appearing in the two-equation model ($\mathbf{D}_{\eta\eta}^{**}, \mathbf{d}_\omega, \alpha^*, \ldots$) are given explicitly as functions of the local-scale properties and some closure variables

$$\mathbf{D}_{\eta\eta}^{**} = \varphi_\eta \{\mathbf{D}_\eta^* \cdot (\mathbf{I} + \nabla \mathbf{b}_{\eta\eta}) - \tilde{\mathbf{v}}_\eta \mathbf{b}_{\eta\eta}\}^\eta \tag{10}$$

$$\mathbf{D}_{\eta\omega}^{**} = \varphi_\eta \{\mathbf{D}_\eta^* \cdot \nabla \mathbf{b}_{\eta\omega} - \tilde{\mathbf{v}}_\eta \mathbf{b}_{\eta\omega}\}^\eta \tag{11}$$

$$\mathbf{D}_{\omega\omega}^{**} = \varphi_\omega \{\mathbf{D}_\omega^* \cdot (\mathbf{I} + \nabla \mathbf{b}_{\omega\omega}) - \tilde{\mathbf{v}}_\omega \mathbf{b}_{\omega\omega}\}^\omega \tag{12}$$

$$\mathbf{D}_{\omega\eta}^{**} = \varphi_\omega \{\mathbf{D}_\omega^* \cdot \nabla \mathbf{b}_{\omega\eta} - \tilde{\mathbf{v}}_\omega \mathbf{b}_{\omega\eta}\}^\omega \tag{13}$$

$$\mathbf{u}_{\eta\eta} = -\mathbf{u}_{\omega\eta} = \mathbf{c}_{\eta\eta} = -\frac{1}{V_\infty} \times \int_{A_{\eta\omega}} \mathbf{n}_{\eta\omega} \cdot (\langle \mathbf{v}\rangle_\eta \mathbf{b}_{\eta\eta} - \mathbf{D}_\eta^* \cdot \nabla \mathbf{b}_{\eta\eta} - \mathbf{D}_\eta^*)\, \mathrm{d}A \tag{14}$$

$$\mathbf{u}_{\omega\omega} = -\mathbf{u}_{\eta\omega} = \mathbf{c}_{\omega\omega} = -\frac{1}{V_\infty} \times \int_{A_{\eta\omega}} \mathbf{n}_{\omega\eta} \cdot (\langle \mathbf{v}\rangle_\omega \mathbf{b}_{\omega\omega} - \mathbf{D}_\omega^* \cdot \nabla \mathbf{b}_{\omega\omega} - \mathbf{D}_\omega^*)\, \mathrm{d}A \tag{15}$$

$$\mathbf{d}_\eta = \varphi_\eta \{\tilde{\mathbf{v}}_\eta r_\eta - \mathbf{D}_\eta^* \cdot \nabla r_\eta\}^\eta \tag{16}$$

$$\mathbf{d}_\omega = -\varphi_\omega \{\tilde{\mathbf{v}}_\omega r_\omega - \mathbf{D}_\omega^* \cdot \nabla r_\omega\}^\omega \tag{17}$$

$$\alpha^* = -\frac{1}{V_\infty} \int_{A_{\eta\omega}} \mathbf{n}_{\eta\omega} \cdot (\langle \mathbf{v}\rangle_\eta r_\eta - \mathbf{D}_\eta^* \cdot \nabla r_\eta)\, \mathrm{d}A + \frac{1}{V_\infty} \int_{A_{\eta\omega}} \mathbf{n}_{\omega\eta} \cdot (\langle \mathbf{v}\rangle_\omega r_\omega - \mathbf{D}_\omega^* \cdot \nabla r_\omega)\, \mathrm{d}A \tag{18}$$

The closure variables, $\mathbf{b}_{\eta\eta}$, $\mathbf{b}_{\omega\omega}$, $\mathbf{b}_{\eta\omega}$, $\mathbf{b}_{\omega\eta}$, r_η, r_ω, are the solutions of three closure problems defined over the unit cell [1].

Problem I

$$\nabla \cdot (\langle \mathbf{v}\rangle_\eta \cdot \mathbf{b}_{\eta\eta}) + \tilde{\mathbf{v}}_\eta = \nabla \cdot (\mathbf{D}_\eta^* \cdot \nabla \mathbf{b}_{\eta\eta}) + \nabla \cdot \widetilde{\mathbf{D}}_\eta^* - \varphi_\eta^{-1} \mathbf{c}_{\eta\eta} \tag{19a}$$

$$B.C.1 \quad \mathbf{b}_{\eta\eta} = \mathbf{b}_{\omega\eta} \quad \text{at } A_{\eta\omega} \tag{19b}$$

$$B.C.2 \quad \mathbf{n}_{\eta\omega} \cdot \mathbf{D}_\eta^* \cdot \nabla \mathbf{b}_{\eta\eta} + \mathbf{n}_{\eta\omega} \cdot \mathbf{D}_\eta^* = \mathbf{n}_{\eta\omega} \cdot \mathbf{D}_\omega^* \cdot \nabla \mathbf{b}_{\omega\eta} \quad \text{at } A_{\eta\omega} \tag{19c}$$

$$\nabla \cdot (\langle \mathbf{v}\rangle_\omega \cdot \mathbf{b}_{\omega\eta}) = \nabla \cdot (\mathbf{D}_\omega^* \cdot \nabla \mathbf{b}_{\omega\eta}) + \varphi_\omega^{-1} \mathbf{c}_{\eta\eta} \tag{19d}$$

$$\text{Periodicity} \quad \mathbf{b}_{\eta\eta}(\mathbf{r} + l_i) = \mathbf{b}_{\eta\eta}(\mathbf{r}), \quad \mathbf{b}_{\omega\eta}(\mathbf{r} + l_i) = \mathbf{b}_{\omega\eta}(\mathbf{r}) \quad i = 1,2,3 \tag{19e}$$

$$\text{Average} \quad \{\mathbf{b}_{\eta\eta}\}^\eta = 0, \quad \{\mathbf{b}_{\omega\eta}\}^\omega = 0 \tag{19f}$$

Problem II

$$\nabla \cdot (\langle \mathbf{v}\rangle_\eta \cdot \mathbf{b}_{\eta\omega}) = \nabla \cdot (\mathbf{D}_\eta^* \cdot \nabla \mathbf{b}_{\eta\omega}) + \varphi_\eta^{-1} \mathbf{c}_{\omega\omega} \tag{20a}$$

$$B.C.1 \quad \mathbf{b}_{\eta\omega} = \mathbf{b}_{\omega\omega} \quad \text{at } A_{\eta\omega} \tag{20b}$$

$$B.C.2 \quad \mathbf{n}_{\eta\omega} \cdot \mathbf{D}_\eta^* \cdot \nabla \mathbf{b}_{\eta\omega} = \mathbf{n}_{\eta\omega} \cdot \mathbf{D}_\omega^* \cdot \nabla \mathbf{b}_{\omega\omega} + \mathbf{n}_{\eta\omega} \cdot \mathbf{D}_\omega^* \quad \text{at } A_{\eta\omega} \tag{20c}$$

$$\nabla \cdot (\langle \mathbf{v}\rangle_\omega \cdot \mathbf{b}_{\omega\omega}) + \tilde{\mathbf{v}}_\omega = \nabla \cdot (\mathbf{D}_\omega^* \cdot \nabla \mathbf{b}_{\omega\omega}) + \nabla \cdot \widetilde{\mathbf{D}}_\omega^* - \varphi_\omega^{-1} \mathbf{c}_{\omega\omega} \tag{20d}$$

$$\text{Periodicity} \quad \mathbf{b}_{\eta\omega}(\mathbf{r} + l_i) = \mathbf{b}_{\eta\omega}(\mathbf{r}), \quad \mathbf{b}_{\omega\omega}(\mathbf{r} + l_i) = \mathbf{b}_{\omega\omega}(\mathbf{r}) \quad i = 1,2,3 \tag{20e}$$

$$\text{Average} \quad \{\mathbf{b}_{\eta\omega}\}^\eta = 0, \quad \{\mathbf{b}_{\omega\omega}\}^\omega = 0 \tag{20f}$$

Problem III

$$\nabla \cdot (\langle \mathbf{v}\rangle_\eta r_\eta) = \nabla \cdot (\mathbf{D}_\eta^* \cdot \nabla r_\eta) - \varphi_\eta^{-1} \alpha^* \tag{21a}$$

$$B.C.1 \quad r_\eta = r_\omega + 1 \quad \text{at } A_{\eta\omega} \tag{21b}$$

$$B.C.2 \quad \mathbf{n}_{\eta\omega} \cdot \mathbf{D}_\eta^* \cdot \nabla r_\eta = \mathbf{n}_{\eta\omega} \cdot \mathbf{D}_\omega^* \cdot \nabla r_\omega \quad \text{at } A_{\eta\omega} \tag{21c}$$

$$\nabla \cdot (\langle \mathbf{v}\rangle_\omega r_\omega) = \nabla \cdot (\mathbf{D}_\omega^* \cdot \nabla r_\omega) + \varphi_\omega^{-1} \alpha^* \tag{21d}$$

$$\text{Periodicity} \quad r_\eta(\mathbf{r} + l_i) = r_\eta(\mathbf{r}), \quad r_\omega(\mathbf{r} + l_i) = r_\omega(\mathbf{r}) \quad i = 1,2,3 \tag{21e}$$

$$\text{Average} \quad \{r_\eta\}^\eta = 0, \quad \{r_\omega\}^\omega = 0 \tag{21f}$$

These problems must be solved on a unit cell representative of the heterogeneous structure. An original numerical procedure has been proposed by Cherblanc et al. [2] able to deal with any double-region geometry. The main strength of the large-scale averaging method is to give an explicit relationship between the local structure and the large-scale properties. This allows one to study precisely how macroscopic properties depend on the local-scale characteristics. Following this idea, sensitivity analysis and discussions can be found in Cherblanc et al. [2].

In order to use the two-equation model with confidence, we need to be able to predict breakthrough curves or concentration fields for any double-permeability system, as complex as required. Since the exchange of mass is a transient phenomena, first-order theories have limitations [2,41,42]. Indeed, the determination of an ''optimal'' mass exchange coefficient will depend on the geometry considered and the boundary conditions imposed as well as the criterion used to define this optimum. Nevertheless, the accuracy of such a model may be sufficient for many practical situation when considering the large number of uncertainties. In this framework, it is interesting to evaluate the impact of these limitations on the ability of the two-equation model to approximate the averaged behavior of two-

region systems. Our objective at this point is to compare solutions of the two-equation model with "numerical experiments", so as to test the theory in the absence of adjustable parameters. The case of stratified systems has been treated in the original paper [1]. For that particular geometry, the large-scale effective properties can be developed analytically. A reasonable agreement was found between large-scale predictions and numerical experiments. In addition, it was found that the asymptotic behavior of the stratified system, which has been described exactly by Marle et al. [73], was also recovered by the proposed theory. The main objective of this paper is to test the theory in the case of more general complex systems.

3. Comparison with numerical experiments

The case of nodules embedded in a continuous matrix (Fig. 2) is presented in this section. Such media are typically double-permeability systems, and can be found in natural formations. Experimental analysis on geological cores have shown sand-shale sequences, where the less permeable zones is materialized by cylindrical inclusions. Permeability ratios between 10^3 and 10^5 are commonly observed [74–76]. Several works have pointed out the relevance of this kind of geometry in geologic structures [46–48,55], which can lead to strongly asymmetric breakthrough curves.

Numerical experiments are carried out to represent as well as possible a one-dimensional tracer experiment on a laboratory column. The heterogeneous sample is composed of twenty nodular unit cells (Fig. 3) aligned along the x-axis. This row pattern is repeated infinitely in the y-direction (Fig. 2). The experiment consists in imposing a constant macroscopic pressure gradient between $x = 0$ and $x = L$, in order to have a steady-state single-phase flow from the left to the right. Then a solute constituent is introduced at the surface $x = 0$. The validation of the proposed theory proceeds in two steps. First, reference solutions are built based on local-scale numerical simulations. Then, after calculation of the "effective properties" on the representative unit cell, the large-scale theoretical predictions are computed, and compared to the numerical experiments.

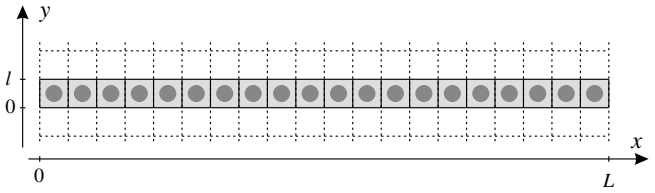

Fig. 2. Periodic nodular system.

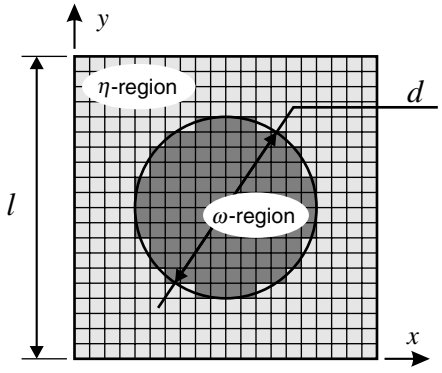

Fig. 3. Two-dimensional nodular unit cell.

3.1. Regional velocities

Using the tracer assumption, which supposes that the single-phase flow is not affected by the presence of a solute constituent, the total mass and momentum balance equations can be solved separately from the tracer dispersion equation. Incidentally, the flow field is considered as a known field in the local-scale description of solute transport (Eqs. (1)–(4)). The first step is to compute the velocity field in the unit cell representative of the periodic nodular system (Fig. 3). This can be done easily using a classical finite volume formulation of the Darcy equation [10,77,78], and this is not further presented here.

An averaging process over the unit cell gives the large-scale regional velocities defined as

$$\{\langle \mathbf{v}\rangle_\eta\}^\eta = \frac{1}{V_\eta}\int_{V_\eta}\langle \mathbf{v}\rangle_\eta \,\mathrm{d}V \quad \text{and}$$
$$\{\langle \mathbf{v}\rangle_\omega\}^\omega = \frac{1}{V_\omega}\int_{V_\omega}\langle \mathbf{v}\rangle_\omega \,\mathrm{d}V \tag{22}$$

Some details about regional velocities can be found in Quintard and Whitaker [79]. Due to the geometrical symmetry of the system and the fact that the main flow is along the x-axis, the y-components of these macroscopic velocities are zero. To simplify the nomenclature, we will use the following notations:

$$v_\eta = (\{\langle \mathbf{v}\rangle_\eta\}^\eta)_x = \|\{\langle \mathbf{v}\rangle_\eta\}^\eta\| \quad \text{and}$$
$$v_\omega = (\{\langle \mathbf{v}\rangle_\omega\}^\omega)_x = \|\{\langle \mathbf{v}\rangle_\omega\}^\omega\| \tag{23}$$

The ratio of these velocities is plotted in Fig. 4 as a function of the permeability ratio for a nodular unit cell. The stratified case is also given for comparison. We observe that for any permeability ratio larger than 10 ($k_\eta/k_\omega \geqslant 10$) and whatever the nodule size, the velocity ratio can be directly estimated from the permeability ratio by

$$\frac{v_\eta}{v_\omega} \approx 0.5\frac{k_\eta}{k_\omega} \tag{24}$$

These large-scale velocities, associated with the convective transport in each region, can give valuable indications for the choice of the model, i.e., "mobile–mobile" vs "mobile–immobile" description. We can fairly consider the low permeability region as "immobile" when the velocity ratio is greater than 100. Consequently, in a nodular structure, "mobile–immobile" descriptions are adequate when

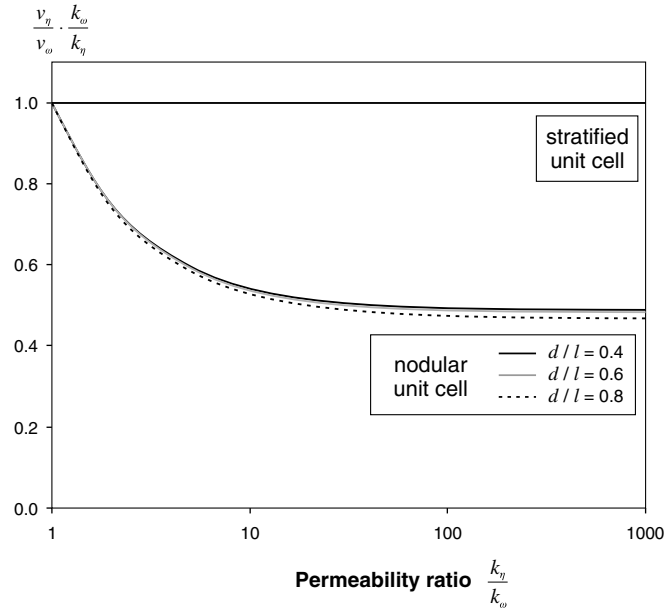

Fig. 4. Velocity ratio as a function of the permeability ratio for stratified and nodular structures.

the permeability ratio is larger than 200. Non-ideal behaviors are also observed when the contrast of permeability takes a lower value. In these situations, classical "mobile–immobile" approaches have often proven to be quite inadequate since convective transport in the low permeability region cannot be neglected. To explore these different situations, three cases are investigated, with permeability ratios k_η/k_ω varying from 10 to 1000.

3.2. Local-scale simulations

The objective of this part is to build some reference solutions based on a fine description of the transport processes through heterogeneities. First, a steady-state single-phase flow from the left to the right is established in the nodular structure (Fig. 2). Then, the surface $x = 0$ is subjected to a sudden change in the local-scale concentration. We choose the following initial and boundary conditions:

$$t = 0,\ \forall x: \quad \langle c\rangle^\beta = 0 \tag{25}$$

$$x = 0,\ \forall t: \quad \langle c\rangle^\beta = 1 \tag{26}$$

$$x = L,\ \forall t: \quad \text{convective flux; } \mathbf{n}\cdot(\mathbf{D}^*_\eta\cdot\nabla\langle c\rangle^\beta) = 0 \tag{27}$$

The Darcy-scale hydrodynamic dispersion tensor is defined according to Bear [64] by the following expression:

Table 1
Local-scale properties of the nodular structure

Unit Cell	l (m)		d (m)	φ_η	L (m)
	0.1		0.06	0.717	2
Physical properties	ε_η	ε_ω	D^{eff} (m s^{-2})	α_L (m)	α_T (m)
	0.4	0.25	10^{-9}	0.002	0.0002

$$\mathbf{D}^*_{ij} = (\alpha_T\|\mathbf{v}\| + D^{\text{eff}})\delta_{ij} + (\alpha_L - \alpha_T)\frac{v_i v_j}{|\mathbf{v}|} \tag{28}$$

where α_L and α_T are the longitudinal and transverse local-scale dispersivities, v_i is a component of the local-scale velocity $\mathbf{v}$ and D^{eff} is the local-scale effective diffusivity. While this is not a limitation of the theory, the medium is considered isotropic for simplicity.

The local properties considered are summarized in Table 1. As discussed in Section 3.1, three cases are investigated, with permeability ratios (k_η/k_ω) varying from 10 to 1000. The dispersive and diffusive characteristics (α_L, α_T and D^{eff}) are chosen identical in both regions. This choice seems to be very restrictive. There is no physical reason to encounter this situation, but, at the large-scale, numerical analysis has shown that the results are not very sensitive to the contrast of dispersive characteristics. Indeed, through Eq. (28), the contrast of dispersive processes between the two regions will be mainly the consequence of the velocity difference, resulting from the permeability contrast. It must be emphasized at this point that this choice of the same dispersivities for both regions is not a limitation of either the theory or the implemented numerical tools.

The macroscopic pressure gradient is chosen to have the norm of the superficial average velocity equal to

$$v = \|\{\langle\mathbf{v}\rangle\}\| = \varphi_\eta v_\eta + \varphi_\omega v_\omega = 10^{-5}\ \text{m s}^{-1} \tag{29}$$

Therefore, the cell Peclet number, as defined in Cherblanc et al. [2], is

$$Pe = \frac{vl}{D^{\text{eff}}} = 1000 \tag{30}$$

Local-scale transport is computed by using the numerical code MT3D [80]. The method of characteristics, free of numerical dispersion, is used for solving the convective transport. An explicit finite-difference scheme is used for the dispersion term. Local-scale simulations are performed using 2000×50 grid blocks, corresponding to one half-row of nodules (Fig. 2). To give a better illustration of the local transport phenomena, the concentration fields are presented on a forty-nodule system by duplicating the simulated row (2000×200 mesh).

For a permeability ratio equal to 100, examples of the local-scale concentration fields obtained from numerical experiments are presented in Fig. 5 at different times. The tracer displacement can be followed from the left to the right. In the matrix (the more permeable zone), convective transport is predominant and responsible for early breakthrough, while slow diffusion occurs in the nodules. The fluctuations of the velocity field inside the more permeable region lead to large-scale dispersion effects and tend to increase the tracer spreading. It must be noticed however that "immobile" zones should not be simply defined by the value of the permeability ratio. Indeed, the regions located between two nodules, where low velocities are observed, behave here as retardation zones. Should the

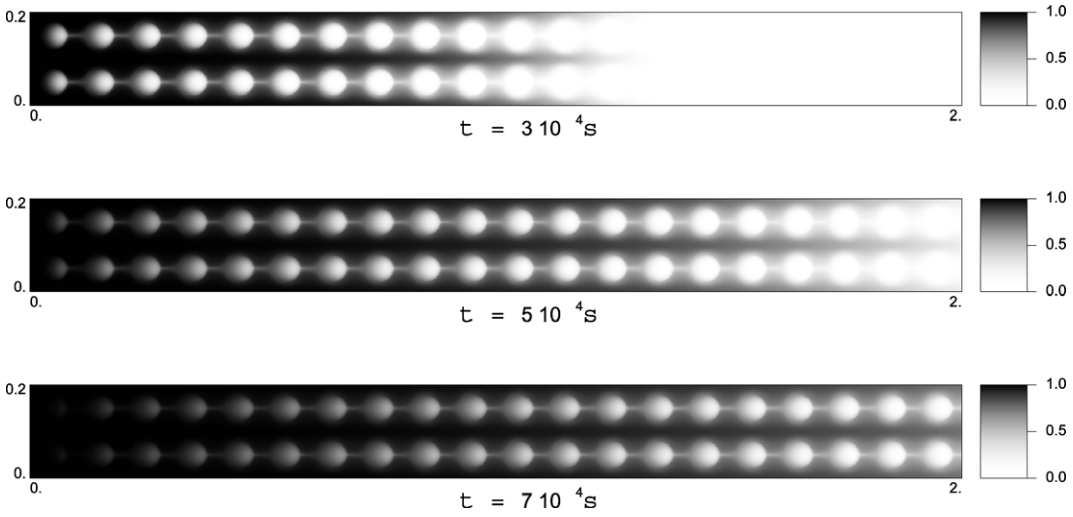

Fig. 5. Concentration fields in the nodular system at different times.

stagnant region in the high-permeability zone be included in the "immobile" zone? So far, we did not explore this idea. The data seems to indicate in our case that the dominant process that leads to non-equilibrium is the mass exchange between the nodules and the continuous region.

To focus on the mass transfer between the nodules and the matrix, some detailed views of the isoconcentrations in the 10th nodules at $t = 4 \times 10^4$ s are plotted in Fig. 6. Three cases are proposed corresponding to different permeability ratios. For low permeability ratio ($k_\eta/k_\omega = 10$), the isoconcentrations clearly reflect the predominance of convective transport crossing over the nodules. We observe some small transversal dispersive effects. On the opposite, with a high permeability ratio ($k_\eta/k_\omega = 1000$), diffusive process is the only significant transport mechanism that takes place within the nodules. In this configuration, mass exchange is fairly approximated by a mixed model based on purely diffusive transport in the inclusions [30–33,81]. Intermediate permeability ratio ($k_\eta/k_\omega = 100$) represent a tricky situation since mass exchange involves both transport mechanisms (convection and dispersion), and neither of them can be neglected. Zinn et al. [56] developed a useful empirical categorization of possible transport regimes for such nodular systems, based on cell Peclet and Damköhler numbers. It confirms that diffusive mass exchange is observed for high permeability ratios, while advective mass transfer is predominant for lower permeability ratios. One interesting feature of the development based on the *volume averaging technique* discussed in this paper is that the closure problem giving the mass exchange coefficient, as well as other effective parameters in the averaged equations, include convective and dispersive transport. In the next section, the calculation of this mass exchange coefficient α^* is presented.

With these computed two-dimensional concentration fields (Fig. 5), large-scale concentrations are built in terms of local volume averages over the unit cell presented in Fig. 3. This leads to the following explicit expressions of the large-scale quantities:

$$\{\langle c\rangle_\eta^\beta\}^\eta = \frac{1}{V_\eta}\int_{V_\eta}\langle c\rangle^\beta \,\mathrm{d}V; \quad \{\langle c\rangle_\omega^\beta\}^\omega = \frac{1}{V_\omega}\int_{V_\omega}\langle c\rangle^\beta \,\mathrm{d}V \tag{31}$$

Here, V_η and V_ω represent the volumes of the η- and ω-region, respectively, contained in the unit cell. Using this

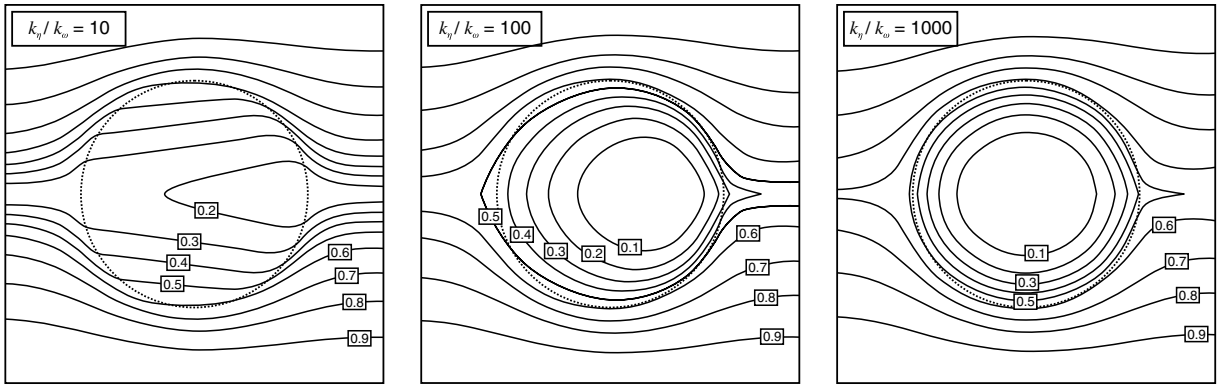

Fig. 6. Isoconcentrations in the 10th nodules at $t = 4 \times 10^4$ s for different permeability ratios.

spatial convolution, the macroscopic transport problem is one-dimensional along the main flow direction (the x-direction in our case). These reference solutions will be called "numerical experiments" in Section 3.5.

3.3. Calculation of large-scale properties

Macroscopic concentration fields are also obtained using the two-equation model (Eqs. (8) and (9)) presented in this work. The first step is to solve the three closure problems (Eqs. (19a)–(21f)) so as to compute the large-scale "effective properties" associated with the nodular unit cell (Fig. 3). Numerical tools have been developed with the ability to deal with a unit cell as complex as necessary. This phase has been extensively described elsewhere [2], and some results are recalled here.

Regarding the case under investigation, all the large-scale effective properties that appear in the two-equation model (Eqs. (8) and (9)) are computed directly from local-scale characteristics. The most important upscaled properties associated with the nodular unit cell described by Fig. 3 and Table 1 are given in Figs. 7 and 8. The large-scale longitudinal dispersion coefficient in the η-region (Fig. 7) and the mass exchange coefficient (Fig. 8) are plotted as functions of the cell Péclet number (Eq. (30)). These coefficients are given for different permeability ratios. Usual behavior is observed for both properties with a diffusive regime at low Peclet number that does not depend on the hydraulic characteristics. For high Peclet number, a linear asymptotic dependence is found ($\propto Pe$).

One must keep in mind that both local-scale transport mechanisms, i.e., convection and dispersion, are taken into account in the theory. It must be emphasized that, so far, theories proposed in the literature have been much more restrictive [22,30,32–35,38–40,53,57,82]. These models cannot be used with complex geometries as they do not take

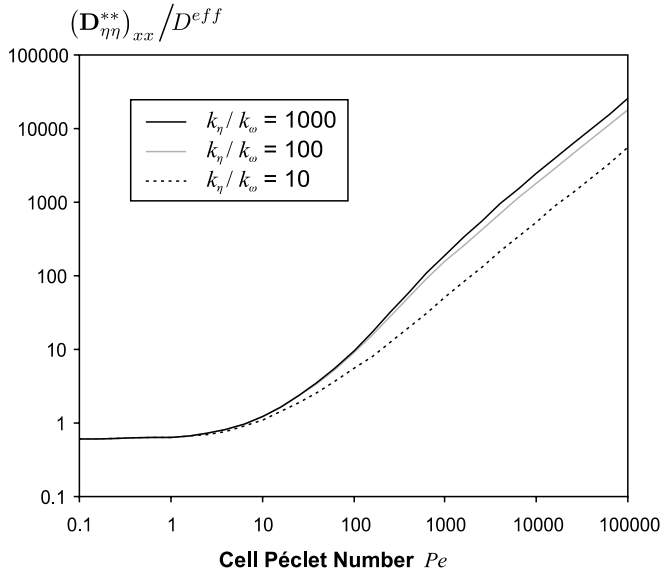

Fig. 7. Large-scale longitudinal dispersion coefficient in the η-region as a function of the cell Péclet number for different permeability ratios.

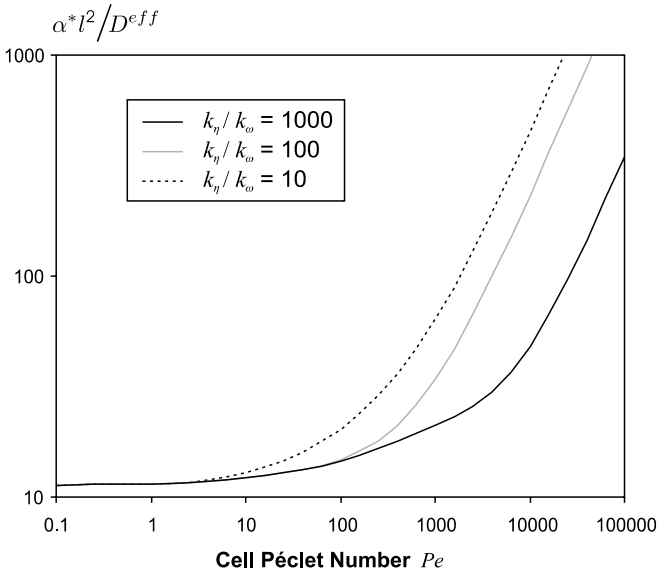

Fig. 8. Large-scale mass transfer coefficient as a function of the cell Péclet number for different permeability ratios.

into account the spatial variations of the local-scale processes (diffusion, dispersion,...). For instance, explicit expressions of the mass exchange coefficient for the nodular configuration are based on a purely diffusive transport in the nodules [30–33,43], and are given by

$$\alpha^* = 32\frac{\varphi_\omega D^{\text{eff}}}{d^2} \tag{32}$$

This is a simple estimate fairly justified for highly contrasted systems ($k_\eta/k_\omega = 1000$ in Fig. 6) or low Peclet numbers (Fig. 8). In all the others situations, convective effects clearly play a dominant role. This is explicitly presented in Fig. 8 through the influence of the Peclet number and the permeability ratio, as the mass exchange coefficient α^* depends more on flow characteristics than on diffusive properties. Details about the comparison between the different proposed estimates of the effective properties and those obtained from the *volume averaging technique* are presented in Cherblanc et al. [2]. This explicit link between scales is one of the major interest of the proposed methodology which allows quantitative understanding of complex, coupled effects, especially in the case of "mobile–mobile" systems.

3.4. Numerical simulation of the two-equation model

Once the computation of macroscopic properties is completed, numerical solutions of the large-scale one-dimensional problem are found by using the following procedure. First, the transport operator is split into two equations as shown here for the η-region equation

$$\varepsilon_\eta\varphi_\eta\frac{\partial}{\partial t}\{\langle c\rangle_\eta^\beta\}^\eta + [\varphi_\eta v_\eta - u_{\eta\eta} - d_\eta]\frac{\partial}{\partial x}\{\langle c\rangle_\eta^\beta\}^\eta + [d_\eta - u_{\eta\omega}]\frac{\partial}{\partial x}\{\langle c\rangle_\omega^\beta\}^\omega = 0 \tag{33}$$

$$\varepsilon_\eta \varphi_\eta \frac{\partial}{\partial t}\{\langle c\rangle_\eta^\beta\}^\eta = D_{\eta\eta}^{**}\frac{\partial^2}{\partial x^2}\{\langle c\rangle_\eta^\beta\}^\eta + D_{\eta\omega}^{**}\frac{\partial^2}{\partial x^2}\{\langle c\rangle_\omega^\beta\}^\omega - \alpha^*(\{\langle c\rangle_\eta^\beta\}^\eta - \{\langle c\rangle_\omega^\beta\}^\omega) \tag{34}$$

As noted previously, the upscaled system is 1D and homogeneous (large-scale properties are constant all over the domain). Thus, only the x-direction components of the two-equation model (Eqs. (8) and (9)) are considered for simulation. Thereby, the quantities $v_\eta, u_{\eta\eta}, d_\eta, \ldots$ correspond to the first component of $\{\langle \mathbf{v}\rangle_\eta\}^\eta, \mathbf{u}_{\eta\eta}, \mathbf{d}_\eta$. The two different transport mechanisms (identified as macroscopic convection, macroscopic diffusion) are separated in order to solve them sequentially. One advantage of this splitting procedure is to handle each equation with an appropriate numerical scheme and a suitable time discretization. The two convection equations like Eq. (33) for the η-region and its equivalent for the ω-region, are coupled. The system can be written as

$$\frac{\partial}{\partial t}\mathbf{C} + \mathbf{V}\frac{\partial}{\partial x}\mathbf{C} = \mathbf{0} \tag{35}$$

$$\mathbf{C} = \begin{bmatrix} \{\langle c\rangle_\eta^\beta\}^\eta \\ \{\langle c\rangle_\omega^\beta\}^\omega \end{bmatrix} \tag{36}$$

$$\mathbf{V} = \begin{bmatrix} \frac{\varphi_\eta v_\eta - u_{\eta\eta} - d_\eta}{\varepsilon_\eta \varphi_\eta} & \frac{d_\eta - u_{\eta\omega}}{\varepsilon_\eta \varphi_\eta} \\ \frac{d_\omega - u_{\omega\eta}}{\varepsilon_\omega \varphi_\omega} & \frac{\varphi_\omega v_\omega - u_{\omega\omega} - d_\omega}{\varepsilon_\omega \varphi_\omega} \end{bmatrix} \tag{37}$$

This system can be decoupled by using a diagonalization decomposition of the matrix $\mathbf{V}$

$$\mathbf{V} = \mathbf{R}\boldsymbol{\Lambda}\mathbf{R}^{-1} \tag{38}$$

This leads to two classical independent convection equations, each associated with a characteristic propagation velocity ($\boldsymbol{\Lambda}$) and a characteristic concentration ($\mathbf{R}^{-1}\mathbf{C}$). In general, the characteristic propagation velocities are different from the large-scale flow velocities

$$\frac{\partial}{\partial t}(\mathbf{R}^{-1}\mathbf{C}) + \boldsymbol{\Lambda}\frac{\partial}{\partial x}(\mathbf{R}^{-1}\mathbf{C}) = \mathbf{0} \tag{39}$$

The resulting convection equations are solved using an explicit second-order TVD scheme [83,84]. The diffusion equations like Eq. (34), are solved using a θ-scheme. The value of θ is $\frac{1}{2}$, which is the value for the Crank–Nicholson method, leading to an unconditionally stable scheme. A CFL condition is required for the resolution of the convection equations. However, the time step can be different while solving diffusion equations. This overall procedure leads to a second-order scheme with negligible numerical dispersion.

We choose the following initial and boundary conditions, which are similar to those imposed at the local-scale (Eqs. (25)–(27))

$$t = 0,\ \forall x: \quad \{\langle c\rangle_\eta^\beta\}^\eta = \{\langle c\rangle_\omega^\beta\}^\omega = 0 \tag{40}$$

$$x = 0,\ \forall t: \quad \{\langle c\rangle_\eta^\beta\}^\eta = \{\langle c\rangle_\omega^\beta\}^\omega = 1 \tag{41}$$

$$x = L,\ \forall t: \quad \text{convective flux;}\ \frac{\partial}{\partial x}\{\langle c\rangle_\eta^\beta\}^\eta = \frac{\partial}{\partial x}\{\langle c\rangle_\omega^\beta\}^\omega = 0 \tag{42}$$

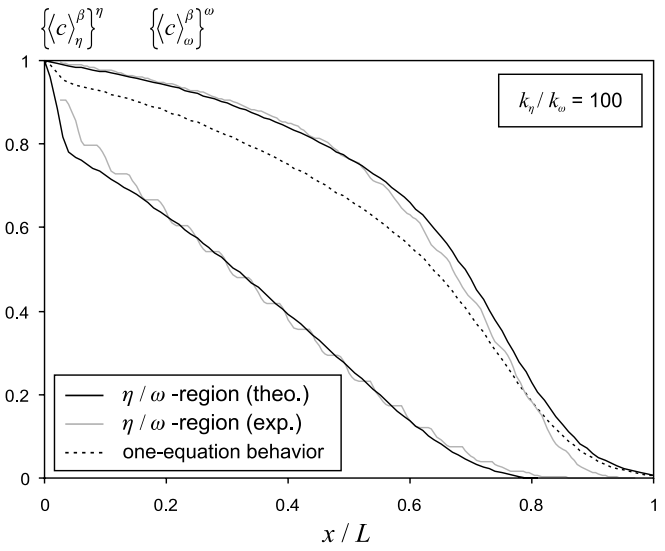

Fig. 9. Comparison between experimental results and theoretical predictions ($t = 4 \times 10^4$ s).

With a low computational cost, large-scale one-dimensional concentration fields are now available, providing theoretical predictions to be compared to the numerical experiments presented in Section 3.2.

3.5. Comparison

In the case of a permeability ratio equal to 100 ($k_\eta/k_\omega = 100$), the large-scale concentration fields obtained for $t = 4 \times 10^4$ s and $t = 6 \times 10^4$ s are plotted in Figs. 9 and 10. The results presented in the next section show that the large-scale mass non-equilibrium is nearly maximum for these times, which means that it is the best situation for testing the two-equation model. One can observe that the theoretical predictions based on Eqs. (8) and (9) are

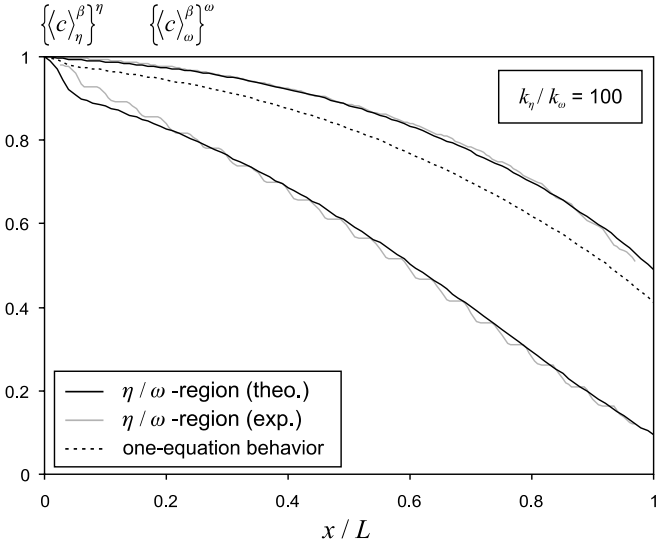

Fig. 10. Comparison between experimental results and theoretical predictions ($t = 6 \times 10^4$ s).

smooth profiles whereas the "experimental" values are subject to fluctuations having a length-scale comparable to the length of a unit cell. This behavior, that results from the volume averaging procedure, has been observed in many situations [85,86], and is discussed by Quintard and Whitaker [87]. Weighting functions can be included in the volume averaging procedure to smooth these results. Despite these fluctuations, the macroscopic experimental behavior can be easily interpreted.

A very good agreement between the numerical experiments and the one-dimensional theoretical predictions is obtained. For systems with a well-connected more permeable region, the existence of preferential flow paths leads to important non-ideal effects. The difference between the transport characteristic times (rapid dominant convection in the matrix – slow diffusion in the nodules) clearly calls for a large-scale non-equilibrium description. In this kind of heterogeneous structures, it is clear that both large-scale transport mechanisms must be taken into account in each region. In general, the assumptions made in "mobile–immobile" models [30,32,35,59,88] may be too drastic.

To be clear about the need of a two-equation model, we also represent the one-equation behavior. The large-scale concentration is calculated using a porosity-weighted average of the concentration in each region [89]

$$C^* = \frac{\varepsilon_\eta \varphi_\eta \{\langle c\rangle_\eta^\beta\}^\eta + \varepsilon_\omega \varphi_\omega \{\langle c\rangle_\omega^\beta\}^\omega}{\varepsilon_\eta \varphi_\eta + \varepsilon_\omega \varphi_\omega} \tag{43}$$

The associated curves are plotted in Figs. 9 and 10. The profile is characteristic of a non-Fickian behavior, and cannot be the solution of a classical advection-dispersion equation. With large-scale mass non-equilibrium effects, a complex one-equation model should be used, such as the formulations proposed in non-local theories [90,91]. A two-domain description allows to increase the degrees of freedom of the model, and can describe most of the large-scale non-equilibrium behavior without adjustable parameters and without a dramatic additional mathematical complexity.

Comparing the outlet concentration curves can also bring some attractive information (Fig. 11). Several definitions of this outlet concentration can be used (surface-, porosity- or velocity-weighted averages, ...). In this work, elution curves based on a velocity-weighted average are calculated, as it corresponds to the concentration measured at the outlet of a laboratory tracer experiment. From fine-grid simulations (Fig. 5), the experimental elution concentration is computed by

$$C_{\text{exp}} = \frac{\int_{A_e} \mathbf{n}_{A_e} \cdot \langle \mathbf{v}\rangle \langle c\rangle^\beta \, \mathrm{d}A}{\int_{A_e} \mathbf{n}_{A_e} \cdot \langle \mathbf{v}\rangle \, \mathrm{d}A} \tag{44}$$

where A_e is the surface perpendicular to the flow at $x = L$ and $\mathbf{n}_{A_e}$ is the corresponding unit normal vector. For such calculations, local-scale simulations are performed using 30 unit cells to avoid the perturbation induced by the diffusive flux boundary condition imposed on the right side of the system (Eq. (27)). At the large scale, a similar definition is chosen for the theoretical elution concentration

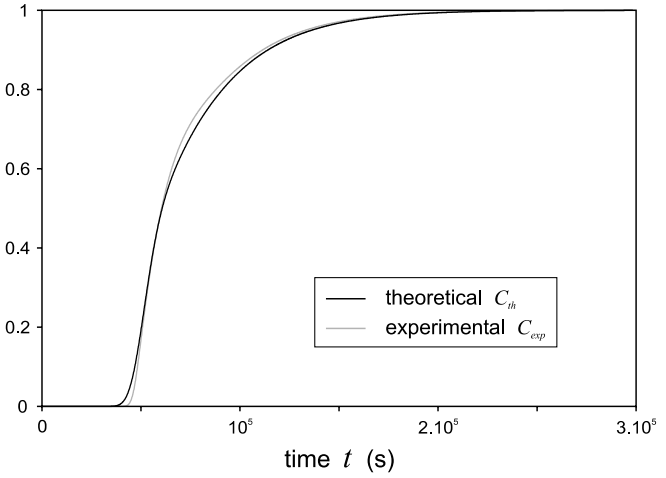

Fig. 11. Comparison between experimental and theoretical elution concentration curves.

$$C_{th} = \frac{\varphi_\eta v_\eta \{\langle c\rangle_\eta^\beta\}^\eta + \varphi_\omega v_\omega \{\langle c\rangle_\omega^\beta\}^\omega}{\varphi_\eta v_\eta + \varphi_\omega v_\omega} \tag{45}$$

where v_η and v_ω correspond to the x-component of $\{\langle \mathbf{v}\rangle_\eta\}^\eta$ and $\{\langle \mathbf{v}\rangle_\omega\}^\omega$. One can note that these local- and large-scale definitions are not mathematically equivalent. Indeed, the theoretical definition (Eq. (45)) using large-scale concentrations involves a spatial average process along the x-direction, whereas the experimental expression (Eq. (44)) is localized at the outlet surface ($x = L$). The discrepancies between them have been estimated to be about a few percent [92]. This point can partly explain the small differences between local- and large-scale elutions curves, as plotted in Fig. 11. Moreover, the volume averaging technique usually under-estimates the mass transfer coefficient α^*, at short times [1,41]. This can be noticed in Figs. 9 and 10 where the experimental non-equilibrium between η- and ω-regions is slightly smaller than the theoretical one. A similar observation is done in Fig. 11 where wee see that, at early time ($t \approx 5 \times 10^4$ s), the theoretical breakthrough occurs before the experimental one. Consequently, the theoretical plume spreading is a little larger. Additional discussions and comparisons based on elution curves, between the two-equation model and experimental simulations are proposed by Golfier et al. [92].

Changing the permeability ratio leads to different macroscopic behaviors, as illustrated in Figs. 12 and 13. For lower permeability contrast ($k_\eta/k_\omega = 10$ in Fig. 12), the large-scale behavior approaches an equilibrium situation, since the mass exchange is enhanced by a high inter-region convective flux (see Fig. 8). Although, large-scale non-equilibrium effects are less important in this case, macroscopic convective transport *must* be taken into account in both regions, justifying a "mobile–mobile" description. Nevertheless, the elution curve could be accurately represented by a one-equation non-equilibrium description [89]. With

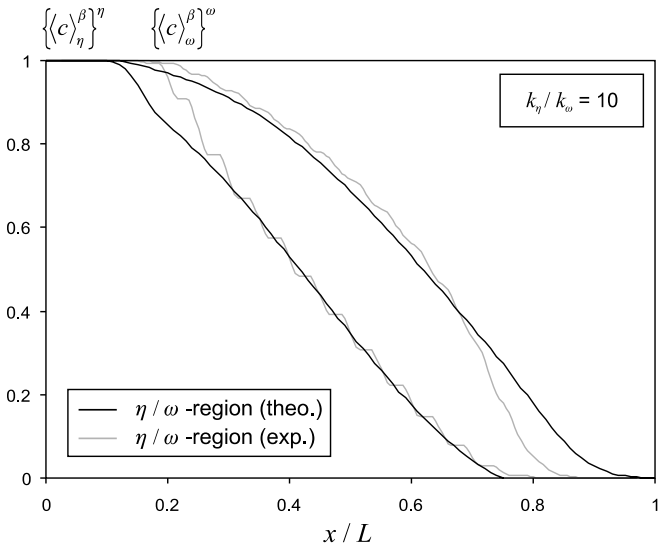

Fig. 12. Comparison between theoretical predictions and experimental results ($t = 4 \times 10^4$ s).

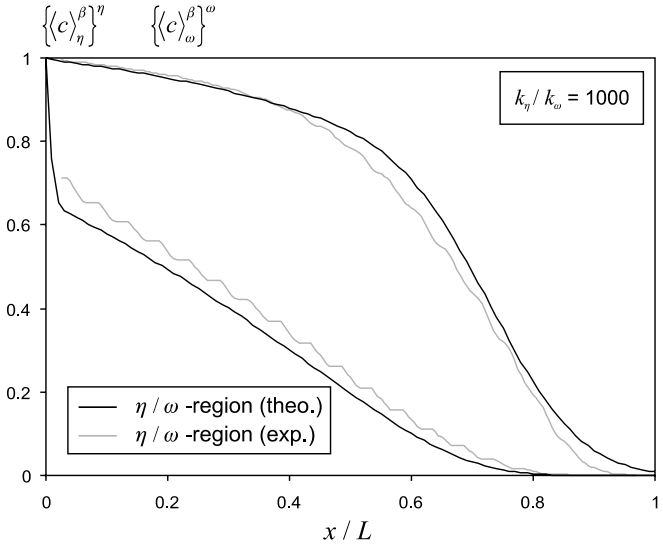

Fig. 13. Comparison between theoretical predictions and experimental results ($t = 4 \times 10^4$ s).

a high permeability contrast ($k_\eta/k_\omega = 1000$ in Fig. 13), the ratio of regional average velocities is around 500 (Fig. 4). Convective transport in the nodules could be neglected, as diffusive processes are predominant. For that class of two-regions systems, non-equilibrium effects are increased, but should be fairly predicted by a "mobile–immobile" representation. In the framework of a first-order kinetic theory to describe the mass exchange between the two regions, the effective mass transfer coefficient, α^*, given by the *volume averaging method* is equal to the harmonic average of the eigenvalues associated with the closure problem [41–43]. Several works have shown that this is the "optimal" value as it assures that the zeroth, first, and second temporal moments of the breakthrough curve are maintained [33,35,43,93]. However, using this "average" value, the mass transfer is under-estimated at short times and over-estimated at long times. In our case ($k_\eta/k_\omega = 1000$ in Fig. 13), the ratio of the characteristic time for diffusion in the inclusions to the characteristic time for convection in the matrix across the system is about 10, which is not so important, accounting for the good agreement we obtained. If the contrast of transport characteristic times increases, a two-equation description based on a first-order mass exchange term may lead to discrepancies, as presented by Golfier et al. [92], and additional developments are necessary to accurately describe these processes. Finally, intermediate values of the permeability ratio, like the first case presented in this section, lead to more complex large-scale behaviors, as none of the local-scale transport mechanisms, namely convection and dispersion, can be neglected. The two-equation models extended to "mobile/mobile" systems offer a more general framework, while being compatible with their "mobile/immobile" counterparts.

We have shown that some confidence can be put on the proposed model, and in the next part, the two-equation model will be used to focus on the non-equilibrium which takes place in nodular systems.

4. Large-scale mass non-equilibrium condition

Large-scale mass non-equilibrium refers to situations in which the term $(\{\langle c\rangle_\eta^\beta\}^\eta - \{\langle c\rangle_\omega^\beta\}^\omega)$ must be kept when developing the large-scale model. This is the case of the two-equation model proposed here. To study the influence of this term, a non-equilibrium criterion is built by integrating the concentration difference over the domain at a given time

$$\Theta(t) = \sqrt{\int_{x=0}^{x=\infty} [C_\eta(t) - C_\omega(t)]^2 \, \mathrm{d}x} \tag{46}$$

$$\text{with} \quad C_\eta = \{\langle c\rangle_\eta^\beta\}^\eta, \quad C_\omega = \{\langle c\rangle_\omega^\beta\}^\omega \tag{47}$$

The system under consideration is constituted by 10^6 nodular unit cells. For the time range and mechanisms considered, this is large enough so that the boundary condition on the right side of the system (Eq. (42)) has no influence on the results. Indeed, this case can be considered as a semi-infinite medium. In Section 3, the limitation to twenty unit cells was essentially due to the high computational cost of fine local-scale simulations used to build the reference solutions. This limitation vanishes as the results presented here come from the 1-D simulation of the *macroscopic two-equation model*.

First, for each set of local-scale characteristics, large-scale properties are computed based on numerical resolution of the closure problems and introduced in the two-equation model. In the second step, the two large-scale one-dimensional concentration fields obtained are integrated over the entire domain to determine the non-equilibrium criterion at a given time (Eq. (46)).

Time-evolution of the non-equilibrium criterion Θ, for different permeability ratios and for different dispersivities are presented in Figs. 14 and 15 respectively. Permeability ratios, between 2 and 1000, have been taken greater that 1 because non-equilibrium effects appear mostly in this case. This point has been documented in the heat transfer case (Fig. 32 in [94]) and observed for transport problems [2]. Other local-scale parameters are taken equal to

$$Pe = 1000, \quad \frac{\alpha_L}{\alpha_T} = 10, \quad \frac{d}{l} = 0.6, \quad \varepsilon_\eta = 0.4, \quad \varepsilon_\omega = 0.25 \tag{48}$$

while $\alpha_L/l = 0.1$ in Fig. 14, and $k_\eta/k_\omega = 100$ in Fig. 15. In each cases, the Damköhler number is given for indication

$$Da = \frac{\alpha^* l}{\{\langle \mathbf{v} \rangle_\eta\}^\eta} \tag{49}$$

One can see in Fig. 14 that non-equilibrium effects increase with the permeability ratio. When computing the flow field, a large contrast of permeability increases the difference of average velocities in each region. If mass exchange is not important enough to homogenize the concentration between the two regions, a higher contrast of convective transport velocities leads actually to greater non-equilibrium effects. On the contrary, when the contrast of permeability is close to 1, the medium can be considered homogeneous and local equilibrium is observed as expected. The results presented in Fig. 15 show that non-equilibrium decreases with high local-scale dispersivities. In this case, local-scale dispersion mechanism increases the mass exchange between the two zones and tends to homogenize the concentration. For very low dispersivities ($\alpha_L/l = 0.01$), the transport problem is close to the purely convective case and non-equilibrium effects are maximum. Similar conclusions have been put forth by Cherblanc et al.

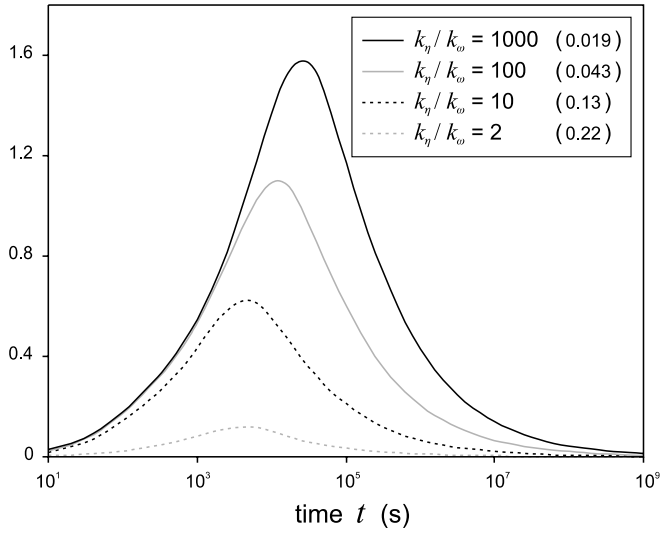

Fig. 14. Evolution of the non-equilibrium criterion as a function of time in a nodular system for different permeability ratios. The Damköhler is given between brackets for indication.

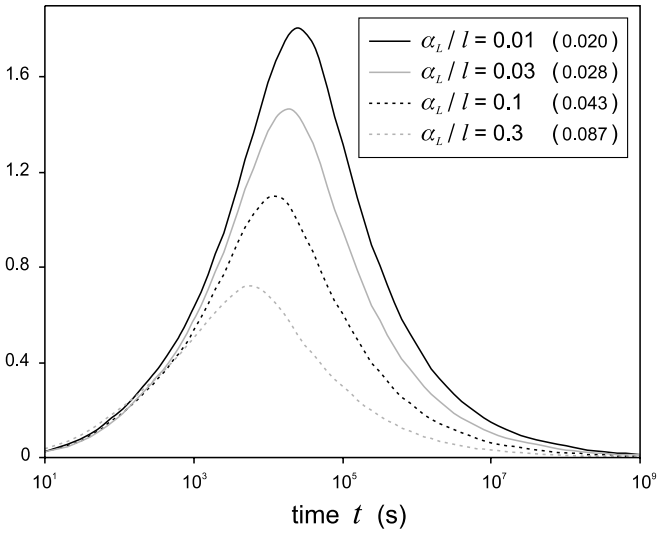

Fig. 15. Evolution of the non-equilibrium criterion as a function of time in a nodular system for different local-scale dispersivities. The Damköhler is given between brackets for indication.

[2], and several works have pointed out the importance of the local-scale dispersion phenomena that can reduce drastically the macro-dispersion [95–97]. For large Peclet numbers, the lower the local-scale dispersion, the greater the non-equilibrium effects and the large-scale dispersion.

For short times, the constraints imposed by the initial boundary condition (Eq. (40)) lead to

$$\Theta(t = 0) = 0 \tag{50}$$

For very long times, non-equilibrium approaches zero

$$\lim_{t \to \infty} \Theta(t) = 0 \tag{51}$$

Whatever the geometry, large-scale mass equilibrium is always satisfied asymptotically, for this initial boundary value problem. This observation reflects the result that the two-equation model converges asymptotically to a one-equation model [1,89,98]. One must keep in mind that this observation may depend on our definition of the non-equilibrium criterion (Eq. (46)). Consequently, a two-equation model is devoid of interest in the asymptotic zone and the macroscopic behavior can be perfectly represented with a *one-equation model*, as discussed in Quintard et al. [89]. However, the choice of the one-equation model and particularly the method to calculate the large-scale dispersion tensor is the major problem. The equilibrium behavior in the asymptotic zone would prompt us to use an equilibrium model. This kind of conclusion is not correct. As defined by Quintard et al. [89], an equilibrium process arises when the exchange coefficient α^* is great enough, so that *at any time*, the two regional averaged concentrations are equal, i.e., $\{\langle c \rangle_\eta^\beta\}^\eta = \{\langle c \rangle_\omega^\beta\}^\omega$. It has been shown in Quintard et al. [89] that the dispersion tensor in the case of a local equilibrium model (according to the above definition) is given by

$$D_{\text{eq}}^{**} = D_{\omega\omega}^{**} + D_{\omega\eta}^{**} + D_{\eta\omega}^{**} + D_{\eta\eta}^{**} \tag{52}$$

It has also been shown that the concentration field obtained with this coefficient does not fit the one obtained from the complete solution of the problem.

The whole transport history must be taken into account when concluding on the validity of the equilibrium assumption. An equilibrium state observed at a given time is not sufficient to characterize an equilibrium process. The non-equilibrium effects, which take place in the pre-asymptotic zone, will considerably increase the global tracer spreading. Within the framework of a one-equation description, the macroscopic longitudinal dispersion coefficient given by a non-equilibrium model is generally greater than the one obtained with an equilibrium representation [2,73,89,99]. Indeed, in this case, the asymptotic dispersion coefficient is given by

$$D_{\infty}^{**} = D_{\eta\eta}^{**} + D_{\omega\omega}^{**} + D_{\eta\omega}^{**} + D_{\omega\eta}^{**} + \frac{1}{\alpha^*}\left(\frac{\varepsilon_\omega\varphi_\omega v_\eta - \varepsilon_\eta\varphi_\eta v_\omega}{\{\varepsilon\}} + u_{\omega\omega} - u_{\eta\eta}\right) \times \left(\frac{\varepsilon_\omega\varphi_\omega v_\eta - \varepsilon_\eta\varphi_\eta v_\omega}{\{\varepsilon\}} + d_\omega - d_\eta\right) \quad (53)$$

and one sees that it depends on the mass exchange coefficient and on the regional velocities. Therefore, non-equilibrium effects *must* be taken into account when calculating macroscopic dispersion coefficients, especially if an apparent dispersion behavior has been reached asymptotically.

The theoretical model and numerical procedures proposed in this work can be considered as tools for the analysis and choice of the model to be used for an accurate description of the macroscopic transport. Indeed, several models are embedded into a single formulation: two-equation model, one-equation non-equilibrium model, equilibrium model. In addition, the proposed generalized two-equation model accounts for ''mobile–immobile'' as well as ''mobile–mobile'' systems.

5. Conclusion

This paper deals with large-scale solute transport in highly heterogeneous systems, where abnormal dispersion is usually observed. This behavior is commonly named ''anomalous'' or ''non-ideal'' referring to the fact that it cannot be represented by the classical advection-dispersion equation valid for homogeneous systems. A typical class of heterogeneous media leading to this macroscopic abnormal behavior is related to double-permeability media. To give prominence to these phenomena, a nodular geometry has been chosen as most of the local-scale processes responsible of anomalous dispersion are represented in such systems, i.e., preferential flow paths, retardation zone, limited mass exchange between zones. So as to have some reference solutions, local-scale numerical simulations based on a detailed description of the heterogeneities have been performed. Using a spatial averaging process over a nodular unit cell, large-scale one-dimensional concentration fields have been built, called ''experimental''. These simulations have shown that both local-scale transport phenomena, convection and dispersion, may play a significant role and should be taken into account when developing a macroscopic theory.

A two-equation model has been developed using the large-scale volume averaging method as proposed in Ahmadi et al. [1]. The main advantage of the theory is that the local problems that are used to calculate the large-scale properties are given explicitly in terms of the local properties, with little simplifications. They incorporate the effects of advection and dispersion in both regions. While limitations of the theory must be kept in mind, this example has shown that even high non-fickian behaviors can be captured for many systems having the structure of double-media.

The numerical tools associated with this theory are briefly presented, and theoretical predictions have been compared favorably to numerical experiments for the nodular case. This comparison clearly shows that two-domain approaches are essential to catch complex large-scale dispersion phenomena, since the mass non-equilibrium cannot be accurately represented by a one-equation description. In some classes of heterogeneous structures, like the nodular case presented here, discrepancies would have been observed with ''mobile–immobile'' models at moderate permeability ratios, suggesting that convection and dispersion must be taken into account when upscaling. This confirms some conclusions put forth in Cherblanc et al. [2] arguing that local dispersion process cannot be neglected when calculating the mass exchange between zones. These encouraging results would suggest to extend this approach to random media. Double-permeability system could be seen as simplified but accurate models of general heterogeneous media generated from statistical characteristics. The ability of the closure problems to link the local-scale to the large-scale, could be used in relation with a geostatistical description of heterogeneities.

Finally, the two-equation model has been used in a numerical analysis of the non-equilibrium that takes place in a semi-infinite nodular system. This mass non-equilibrium shows a maximum for intermediate times before going to zero for long times. In the asymptotic region, the two-equation model converges to a one-equation model, which *does not* correspond to the so-called local equilibrium model. As presented in Quintard et al. [89], an asymptotic one-equation model must incorporate the tracer history through the non-equilibrium that takes place before the asymptotic regime. The proposed model can be useful to discuss the validity of the large-scale mass equilibrium assumption, and predict when non-ideal effects appear.

References

[1] Ahmadi A, Quintard M, Whitaker S. Transport in chemically and mechanically heterogeneous porous media V: two-equation model for solute transport with adsorption. Adv Water Resour 1998;22:59–86.

[2] Cherblanc F, Ahmadi A, Quintard M. Two-medium description of dispersion in heterogeneous porous media: calculation of macroscopic properties. Water Resour Res 2003;39:1154–73.
[3] Gelhar LW, Axness CL. Three-dimensional stochastic analysis of macrodispersion in aquifers. Water Resour Res 1983;19:161–80.
[4] Dagan G. Transport in heterogeneous porous formations: spatial moments, ergodicity, and effective dispersion. Water Resour Res 1990;26:1281–90.
[5] Graham WD, McLaughlin DB. A stochastic model of solute transport in groundwater: application to the Borden, Ontario, tracer test. Water Resour Res 1991;27:1345–59.
[6] Fiori A. The relative dispersion and mixing of passive solutes in transport in geologic media. Transp Porous Media 2001;42:69–83.
[7] Zhang D. Stochastic methods for flow in porous media: coping with incertainties. San Diego, CA: Academic Press; 2002.
[8] Wood B, Cherblanc F, Quintard M, Whitaker S. Volume averaging for determining the effective dispersion tensor: closure using periodic unit cells and comparisons with ensemble averaging theory. Water Resour Res 2003;39:1210–31.
[9] Matheron G. Eléments pour une théorie des milieux poreux, Masson et Cie, 1967.
[10] Quintard M, Whitaker S. Ecoulement monophasique en milieu poreux: effet des hétérogénéités locales. J Méc Théor Appl 1987;6:691–726.
[11] Dagan G. Flow an transport in porous formations. New York: Springer-Verlag; 1989.
[12] King PR. The use of renormalization for calculating effective permeability. Transp Porous Media 1989;4:37–58.
[13] Renard P, de Marsiliy G. Calculating equivalent permeability: a review. Adv Water Resour 1997;20:253–78.
[14] Brusseau ML, Rao PSC. Non-equilibrium and dispersion during transport of contaminants in groundwater: field-scale process. Contaminant transport in groundwater. Rotterdam: Balkema; 1989. p. 237–44.
[15] Herr M, Schäfer G, Spitz K. Experimental studies of mass transport in porous media with local heterogeneities. J Contam Hydrol 1989;4:127–37.
[16] Berkowitz B, Scher H. On characterization of anomalous dispersion in porous and fractured media. Water Resour Res 1995;31:1461–6.
[17] Pickens JF, Grisak GE. Scale-dependent dispersion in a stratified granular aquifer. Water Resour Res 1981;17:1191–211.
[18] Dagan G. Time-dependent macrodispersion for solute transport in anisotropic heterogeneous aquifers. Water Resour Res 1988;24:1491–500.
[19] Gelhar LW, Welty C, Rehfeldt KR. A critical review of data on field-scale dispersion aquifers. Water Resour Res 1992;28:1955–74.
[20] Logan JD. Solute transport in porous media with scale-dependent dispersion and periodic boundary conditions. J Hydrol 1996;184:261–76.
[21] Harvey CF, Gorelick SM. Rate-limited mass transfer or macrodispersion: which dominates plume evolution at the macrodispersion experiment (made) site? Water Resour Res 2000;36:637–50.
[22] Brusseau ML, Jessup RE, Rao PSC. Modeling the transport of solutes influenced by multiprocess non-equilibrium. Water Resour Res 1989;25:1971–88.
[23] Fesch C, Simon W, Haderlein S, Reichert P, Schwarzenbach R. Nonlinear sorption and nonequilibrium solute transport in aggregated porous media: experiments, process identification and modeling. J Contam Hydrol 1998;31:373–407.
[24] Quintard M, Whitaker S. Transport in chemically and mechanically heterogeneous porous media IV: large-scale mass equilibrium for solute transport with adsorption. Adv Water Resour 1998;22:33–58.
[25] Goltz MN, Roberts PV. Interpreting organic solute transport data from a field experiment using physical non-equilibrium models. J Contam Hydrol 1986;1:77–93.
[26] Bajracharya K, Barry DA. Nonequilibrium solute transport parameters and their physical significance: numerical and experimental results. J Contam Hydrol 1997;24:185–204.
[27] Larsson M, Jarvis N. Evaluation of a dual-porosity model to predict field-scale solute transport in a macroporous soil. J Hydrol 1999;215:153–71.
[28] Feehley C, Zheng C, Molz F. A dual-domain mass transfer approach for modeling solute transport in heterogeneous aquifers: application to the macrodispersion experiment (MADE) site. Water Resour Res 2000;36:2501–15.
[29] Sánchez-Vila X, Carrera J. On the striking similarity between the moments of breakthrough curves for a heterogeneous medium and a homogeneous medium with a matrix diffusion term. J Hydrol 2003;294:164–75.
[30] Van Genuchten MT, Wierenga PJ. Mass transfer studies in sorbing porous media i. analytical solutions. Soil Sci Soc Am J 1976;40:473–80.
[31] Van Genuchten MT, Tang DH, Guennelon R. Some exact solutions for solute transport through soils containing large cylindrical macropores. Water Resour Res 1984;20:335–46.
[32] Goltz MN, Roberts PV. Three-dimensional solutions for solute transport in an infinite medium with mobile and immobile zones. Water Resour Res 1986;22:1139–48.
[33] Parker JC, Valocchi AJ. Constraints on the validity of equilibrium and first-order kinetic transport models in structured soils. Water Resour Res 1986;22:399–407.
[34] De Smedt F, Wierenga PJ. Mass transfer in porous media with immobile water. J Hydrol 1979;41:59–67.
[35] Rao PSC, Jessup RE, Rolston DE, Davidson JM, Kilcrease DP. Experimental and mathematical description of nonadsorbed solute transfer by diffusion in spherical aggregates. Soil Sci Soc Am J 1980;44:684–8.
[36] Rao P, Rolston D, Jessup R, Davidson J. Solute transport in aggregated porous media: theoretical and experimental evaluation. Soil Sci Soc Am J 1980;44:1139–46.
[37] Rao P, Jessup R, Addiscott T. Experimental and theoretical aspects of solute diffusion in spherical and nonspherical aggregates. Soil Sci 1982;133:342–9.
[38] Gvirtzam H, Paldor N, Magaritz M, Bachmat Y. Mass exchange between mobile freshwater and immobile saline water in the unsaturated zone. Water Resour Res 1988;24:1638–44.
[39] Zurmühl T, Durner W. Modeling transient water and solute transport in a biporous soil. Water Resour Res 1996;32:819–29.
[40] Gwo J, Jardine P, Wilson G, Yeh G. Using a multiregion model to study the effects of advective and diffusive mass transfer on local physical non-equilibrium and solute mobility in a structured soil. Water Resour Res 1996;32:561–70.
[41] Landereau P, Noetinger B, Quintard M. Quasi-steady two-equation models for diffusive transport in fractured porous media: large-scale properties for densely fractured systems. Adv Water Resour 2001;24:863–76.
[42] Haggerty R, Gorelick S. Multiple-rate mass transfer for modeling diffusion and surface reactions in media with pore-scale heterogeneity. Water Resour Res 1995;31:2383–400.
[43] Haggerty R, McKenna S, Meigs L. On late-time behavior of tracer test breakthrough curves. Water Resour Res 2000;36:3467–79.
[44] Dentz M, Berkowitz B. Transport behavior of a passive solute in continuous time random walks and multirate mass transfer. Water Resour Res 2003;39:1111. doi:10.1029/2001WR001163.
[45] Schumer R, Benson DA, Meerschaert MM, Baeumer B. Fractal mobile/immobile solute transport. Water Resour Res 2003;39:1296. doi:10.1029/2003WR002141.
[46] Guswa A, Freyberg D. Slow advection and diffusion through low permeability inclusions. J Contam Hydrol 2000;46:205–32.
[47] Dagan G, Lessoff S. Solute transport in heterogeneous formations of bimodal conductivity distribution. 1 theory. Water Resour Res 2001;37:465–72.

[48] Lessoff S, Dagan G. Solute transport in heterogeneous formations of bimodal conductivity distribution. 2 applications. Water Resour Res 2001;37:473–80.
[49] Skopp J, Gardner WR, Tyler EJ. Solute movement in structured soils: two-region model with small interaction. Soil Sci Soc Am J 1981;45:837–42.
[50] Dykhuizen RC. A new coupling term for dual-porosity models. Water Resour Res 1990;26:351–6.
[51] Gerke HH, Van Genuchten MT. A dual-porosity model for simulating the preferential movement of water and solutes in structured porous media. Water Resour Res 1993;29:305–19.
[52] Gerke HH, Van Genuchten MT. Macroscopic representation of structural geometry for simulating water and solute movement in dual-porosity media. Adv Water Resour 1996;19:343–57.
[53] Gwo J-P, O'Brien R, Jardine PM. Mass transfer in structured porous media: embedding mesoscale structure and microscale hydrodynamics in a two-region model. J Hydrol 1998;208: 204–22.
[54] Vogel T, Gerke H, Zhang R, Genuchten MV. Modeling flow and transport in a two-dimensional dual-permeability system with spatially variable hydraulic properties. J Hydrol 2000;238:78–89.
[55] Zinn B, Harvey C. When good statistical models of aquifer heterogeneity go bad: a comparison of flow, dispersion, and mass transfer in connected and multivariate gaussian hydraulic conductivity fields. Water Resour Res 2003;39:1051. doi:10.1029/2001WR001146.
[56] Zinn B, Meigs L, Harvey C, Haggerty R, Peplinski W, Schwerin CV, et al. Experimental visualisation of solute transport and mass transfer processes in two-dimensional conductivity fields with connected regions of high conductivity. Environ Sci Technol 2004;38:3916–26.
[57] Van Genuchten MT, Dalton FN. Models for simulating salt movement in aggregated field soils. Geoderma 1986;38:165–83.
[58] Schwarze H, Jaekel U, Vereecken H. Estimation of macrodispersion by different approximation methods for flow and transport in randomly heterogeneous media. Transp Porous Media 2001;43:265–87.
[59] Gaudet JP, Jégat H, Vachaud G, Wierenga PJ. Solute transfer, with exchange between mobile and stagnant water, through unsaturated sand. Soil Sci Soc Am J 1977;41:665–71.
[60] Grisak GE, Pickens JF. Solute transport through fractured media 1. The effect of matrix diffusion. Water Resour Res 1980;16:719–30.
[61] Goltz MN, Roberts PV. Simulations of physical nonequilibrium solute transport models: application to a large-scale field experiment. J Contam Hydrol 1988;3:37–63.
[62] Maraga M. Prediction of mass-transfer coefficient for solute transport in porous media. J Contam Hydrol 2001;50:1–19.
[63] Johnson G, Gupta K, Putz D, Huc Q, Brusseau M. The effect of local-scale physical heterogeneity and nonlinear, rate-limited sorption/desorption on contaminant transport in porous media. J Contam Hydrol 2003;64:35–58.
[64] Bear J. On the tensor form of dispersion in porous media. J Geophys Res 1961;66:1185–97.
[65] Combarnous MA, Fried JJ. Dispersion in porous media. Adv Hydrosci 1971;7:169–282.
[66] Passioura JB. Hydrodynamic dispersion in aggregated media. Soil Sci 1971;111:339–44.
[67] Quintard M, Whitaker S. Transport in ordered and disordered porous media III: closure and comparison between theory and experiment. Transp Porous Media 1994;15:31–49.
[68] Gray WG. A derivation of the equations for multi-phase transport. Chem Eng Sci 1975;30:229–33.
[69] Quintard M, Whitaker S. Two-phase flow in heterogeneous porous media: the method of large-scale averaging. Transp Porous Media 1988;3:357–413.
[70] Quintard M, Whitaker S. Transport in ordered and disordered porous media: volume-averaged equations, closure problems, and comparison with experiment. Chem Eng Sci 1993;48:2537–64.
[71] Ahmadi A, Quintard M. Large-scale properties for two-phase flow in random porous media. J Hydrol 1996;183:69–99.
[72] Pickup G, Ringrose P, Jensen J, Sorbie K. Permeability tensors for sedimentary structures. Math Geol 1994;26:227–50.
[73] Marle CM, Simandoux P, Pacsirszky J, Gaulier C. Etude du déplacement de fluides miscibles en milieu poreux stratifié. Rev l'Institut Fran Pétrole 1967;22:272–94.
[74] Kramers JW, Bachu S, Cuthiell DL, Prentice ME, Yuan LP. A multidisciplinary approach to reservoir characterization: the Provost Upper Mannville B Pool. J Canad Petrol Technol 1989;28:48–57.
[75] Bachu S, Cuthiell D. Effects of core-scale heterogeneity on steady state and transient fluid flow in porous media: numerical analysis. Water Resour Res 1990;26:863–74.
[76] Desbarats AJ. Macrodispersion in sand-shale sequences. Water Resour Res 1990;26:153–63.
[77] Aziz K, Settari A. Petroleum reservoir simulation. London: Applied Science Publishers; 1979.
[78] Fabrie P, Quintard M, Whitaker S. Calculation of porous media effective properties: computational problems and required unit cell features. Mathematical modeling of flow through porous media. London: World Scientific Publishing Co; 1995. p. 166–82.
[79] Quintard M, Whitaker S. Transport in chemically and mechanically heterogeneous porous media III: large-scale mechanical equilibrium and the regional form of Darcy's law. Adv Water Resour 1998;21:617–29.
[80] Zheng C. MT3D: A modular three-dimensional transport model for simulation of advection, dispersion and chemical reactions of contaminants in groundwater systems. S.S. Papadopulos and Associates, Inc.; 1994.
[81] De Smedt F, Wierenga PJ. A generalized solution for solute flow in soils with mobile and immobile water. Water Resour Res 1979;15:1137–41.
[82] Gerke HH, Van Genuchten MT. Evaluation of a first-order water transfer term for variably saturated dual-porosity flow models. Water Resour Res 1993;29:1225–38.
[83] Tackacs LL. A two-step scheme for the advection equation with minimized dissipation and dispersion errors. Mon Weather Rev 1985;113:1050–65.
[84] Bruneau C, Fabrie P, Rasetarinera P. An accurate finite difference scheme for solving convection-dominated diffusion equations. Int J Numer Methods Fluids 1997;24:169–83.
[85] Prat M. On the boundary conditions at the macroscopic level. Transp Porous Media 1989;4:259–80.
[86] Prat M. Some refinements concerning the boundary conditions at the macroscopic level. Transp Porous Media 1992;7: 147–61.
[87] Quintard M, Whitaker S. Transport in ordered and disordered porous media I: the cellular average and the use of weighting functions. Transp Porous Media 1994;14:163–77.
[88] Brusseau ML, Gerstl Z, Augustijn D, Rao PSC. Simulating solute transport in an aggregated soil with the dual-porosity model: measured and optimized parameter values. J Hydrol 1994;163:187–93.
[89] Quintard M, Cherblanc F, Whitaker S. Dispersion in heterogeneous porous media: one-equation non-equilibrium model. Transp Porous Media 2001;44:181–203.
[90] Koch DL, Brady JF. A non-local description of advection–diffusion with application to dispersion in porous media. J Fluid Mech 1987;180:387–403.
[91] Cushman JH, Ginn TR. Nonlocal dispersion in media with continuously evolving scales of heterogeneity. Transp Porous Media 1993;13:123–38.
[92] Golfier F, Quintard M, Cherblanc F, Harvey C, Zinn B, Wood B, et al. Solute transport in highly heterogeneous porous media. Adv Water Resour, submitted for publication.
[93] Harvey C, Gorelick S. Temporal moment-generating equations: modeling transport and mass transfer in heterogeneous aquifers. Water Resour Res 1995;31:1895–911.

[94] Quintard M, Whitaker S. One- and two-equation models for transient diffusion processes in two-phase systems. Advances in heat transfer. New York: Academic Press; 1993. p. 369–464.
[95] Andricevic R. Effects of local dispersion and sampling volume on the evolution of concentration fluctuations in aquifers. Water Resour Res 1998;34:1115–29.
[96] Fiori A. On the influence of pore-scale dispersion in nonergodic transport in heterogeneous formations. Transp Porous Media 1998;30:57–73.
[97] Fiori A. On the influence of local dispersion in solute transport through formations with evolving scales of heterogeneity. Water Resour Res 2001;37:235–42.
[98] Zanotti F, Carbonell RG. Development of transport equations for multiphase systems I: general development for two-phase systems. Chem Eng Sci 1984;39:263–78.
[99] Lake LW, Hirasaki GJ. Taylor's dispersion in stratified porous media. SPE J 1981:459–68.